# Evidence of a Several-Day Propagating Wave

CLAUDE MILLOT

*Laboratoire d'Océanographie Physique du Muséum, Antenne de Toulon, 83501-La Seyne, France*

(Manuscript received 18 September 1983, in final form 28 November 1984)

ABSTRACT

A large 8-day oscillation was recorded during several months by current meters moored at several depths and places on the continental slope, off the Gulf of Lions in the northwestern Mediterranean Sea. This signal is clearly associated with a propagating wave. The location of the moorings, the space and time scale and specific features of the signal account for a relationship between the characteristics of the wave and the mean bottom slope. As supported by the results of a simple analytical model, it is suggested that the bottom slope acts like a wave-guide for the wave.

## 1. Introduction

In the 1970s, several experiments were conducted on the continental shelf of the Gulf of Lions (coastal upwelling and inertial oscillations studies; Millot, 1981) and farther offshore (deep water formation studies; Gascard, 1977), but little attention was paid to the continental slope zone (Fig. 1). Since 1980, current measurements have been made at various depths and places, between the 500 and 2000 m isobaths. In the northwestern Mediterranean Sea, the main large scale hydrodynamical phenomenon is the Ligurian Current which flows westwards along the coast of Provence (Fig. 2). West of 5°30'E, shallow waters tend to penetrate onto the continental shelf (Millot and Wald, 1980), but the core of the current roughly follows the shelf break to the southwest (Fieux, 1972). Thus, the Ligurian Current separates the continental shelf waters from the offshore ones; the later, in a region of ~80 km around the point 42°N, 5°E, are characterized by a weak mean flow and a weak stratification linked to the bowing path of the current (doming structure).

Two current records, obtained at A and B near the bottom in the homogeneous and quiet area (Fig. 3), undoubtedly reveal the occurrence for about 4 months of a long-period wave. Specific features as for instance turnings associated with speed extrema, give information on the proper structure of the wave. Spectral analysis technics were applied to statistically define the period (~8 days) and the phase lag between the records. Therefore, a large part of this paper is devoted to the analysis of the wave itself (Section 2). The characteristics of the wave account for a significant influence of the bottom topography; indeed, as supported by simple computations (Section 3), the bottom slope can act like a wave-guide for such a wave. One of the possible mechanisms is that a wave, generated along the coast of Provence through instability of the Ligurian Current, is trapped by the bottom slope and deflected southwestward in the quiet area. But available measurements are not sufficient to accurately analyze the unstability processes that probably affect this current system.

## 2. The observations

The PROFANS experiment was conducted by two laboratories associated with the CNRS. Two current meters were moored at points A and B (Figs. 2, 3), at 10 m above the bottom on the 1790 m isobath from late August 1980 to mid-March 1981. The data obtained until the end of December are the foundations of the present paper. The points are plotted on a Seabeam bathymetric chart (Fig. 4) which was not available in August 1980; A is inside and B is outside of the canyon (as defined in the caption of Fig. 4), at about 6.2 km apart in the 245°T direction. As shown next, the records are obviously influenced by the local bathymetry; but no observed phenomena has been related to the proper dynamics of the canyon (Millot and Monaco, 1984). The sampling interval was ½ hour.

The progressive vector diagrams (Fig. 5a, b) reveal that the 4-month mean directions are ~200°T at A and 280°T at B; this characteristic is related to bottom features, the length scale of which is several kilometers (Fig. 4). The net virtual displacements are ~380 km at A and 300 km at B, leading to net mean speeds of ~3.3 and 2.6 cm $s^{-1}$. Nearly all the similarities and differences between the records, hereafter emphasized, will be interpreted later.

The progressive vector diagram at A (Fig. 5a) presents a stair-like structure which is not so obvious at B (Fig. 5b). Nevertheless, such a structure is displayed at both points by the direction-histograms

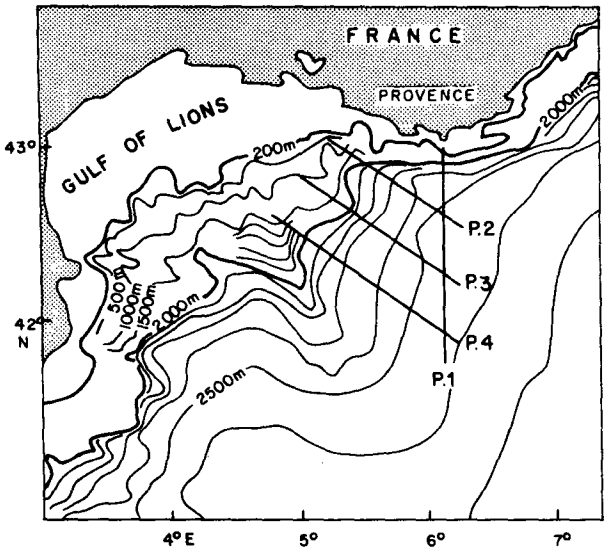


FIG. 1. General bathymetric chart of the northwestern Mediterranean Sea. The large extension of the deep-sea fan, in the axis of which current meters A and B were moored, is to be noticed. P1, . . . , P4 indicate bathymetric profiles considered in Section 2b.

(Fig. 6a): at A, the broad peak results from the juxtaposition of a large peak centered at 220°T and a narrow one centered at 150°T (70° apart), while at B, a larger peak is observed at 290°T and a smaller one at 210°T (80° apart); the values at A are more concentrated in the peaks than at B. The speed histograms at A and B (Fig. 6b) display averaged values of 5.16 and 4.63 cm $s^{-1}$, and maxima of ~17 and 21 cm $s^{-1}$ (~14 and 17 cm $s^{-1}$ when the inertial currents are filtered out); at A, a peak is centered at 4–5 cm $s^{-1}$ while at B, a narrower peak is observed at lower values (3 cm $s^{-1}$) and lower and higher values are more frequent.

The rocking motion observed at A, and displayed by the time series of the direction (Fig. 7a) is associated with a speed modulation (Fig. 7b): a several-day signal appears on both parameters. The low-frequency speed presents smooth sinusoidal variations between 0 and 10 cm $s^{-1}$. On the other hand, the direction is sometimes rather constant (30 November–3 December for instance), sometimes slowly varying (3–5 December) and sometimes quickly turning clockwise by almost 90° (17 December); a striking feature is that

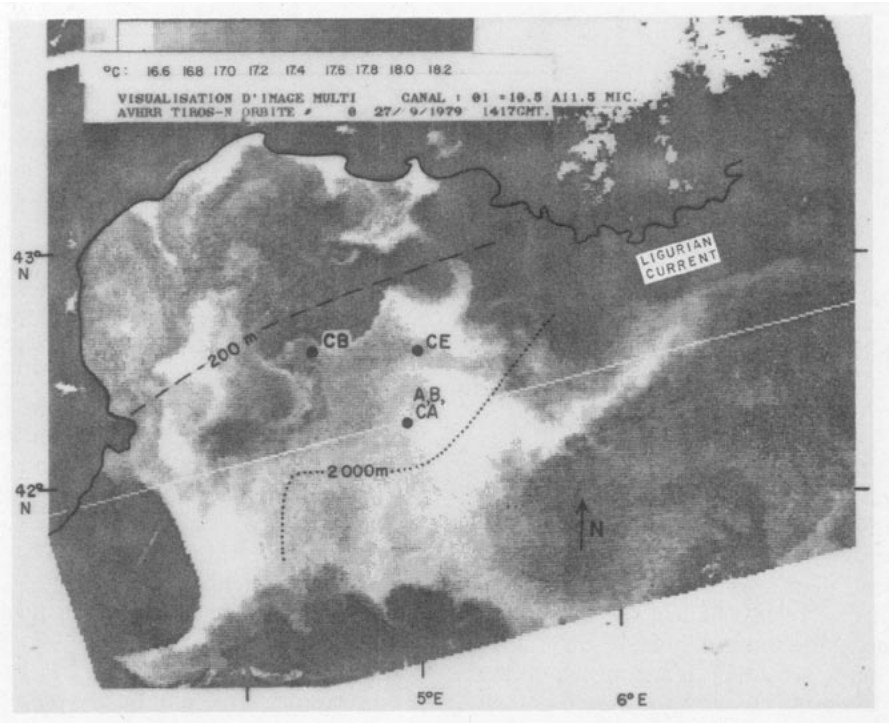


FIG. 2. The warm waters observed along the coast of Provence and along the 200 m isobath in the Gulf of Lions materialize the Ligurian Current. Strong northwesterlies, blowing for several days mainly in the gulf, erode the forepart of the current (Millot and Wald, 1980) and waters are upwelled in a limited number of coastal source points (Millot, 1978). The doming structure linked to the bowing path of the Ligurian Current is revealed by the cold waters encountered near 42°N, 5°E. The overall warmer waters are frequently observed near the southwestern edge of the gulf in relation with the windscreen action of the Pyrenees chain. The large distance between points A, B and CA and the offshore edge of the Ligurian Current is to be noticed.

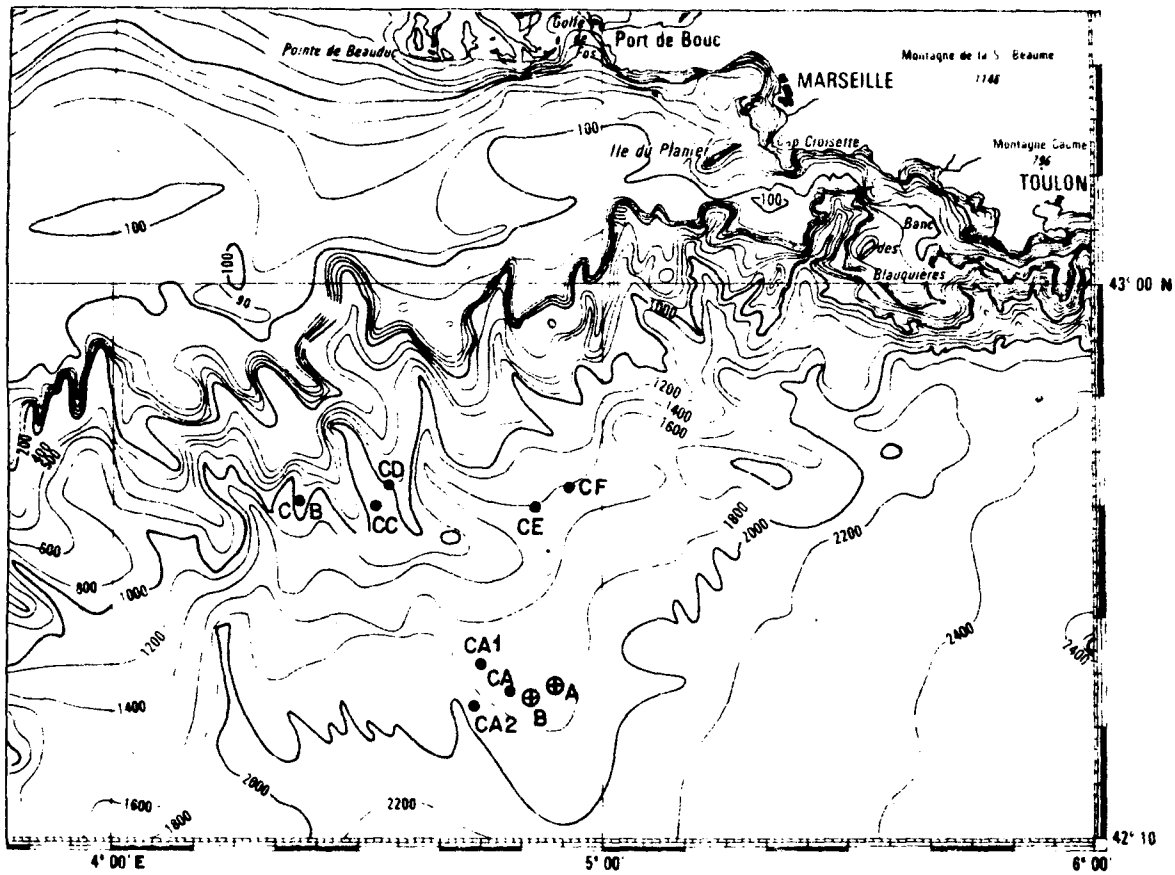


FIG. 3. The upper part of the continental slope is cutted by numerous canyons, but the lower part is rather smooth. All the records collected at the various locations were examined.

this rapid turning frequently occurs with large speeds. At B such an oscillation does not appear on the time series of the direction (Fig. 7c), but complete rotations of the current are frequently observed (4 December); the speed (Fig. 7d) oscillates, but the period is not defined.

The pieces of the progressive vector diagrams drawn in Fig. 8 are representative of the phenomena observed at the two points during the entire studied period. Schematically at A (starting for instance on 19 December), the speed decreases and the current slowly turns to the left in a few days. Then, for several days, the speed increases, the current quickly turns to the right in a few hours and the cycle begins again. At B (starting on 20 December), the speed decreases and the current slowly turns to the left in a few days too, but this latter phase of the cycle may be replaced by a complete rotation to the right (15 December). Then, for only 1 or 2 days, the speed increases, the current quickly turns to the right and keeps for several days this new direction which ends the cycle.

Considering the rapid clockwise turnings observed at A, similar features, even less systematic, occur at B with a time lag ranging from several hours to a few days (for instance, on 17 December at noon at A, and on 18 December at 0600 LST at B), (Fig. 8). This fact supports the hypothesis of a unique phenomenon, but the directions of the mean currents at A and B, which differ by almost 80°, certainly distort the perception of this phenomenon. Therefore, interesting results are expected from comparisons between the plots of the components which are only shifted by their mean value (Fig. 9). The occurrence of a several-day oscillation is now obvious; a visual analysis of the whole records leads to a mean period of ~8 days and a mean time lag of 0.5–1 day. Nevertheless, the detailed analysis made in the previous paragraphs was necessary 1) to emphasize the effect of the mean local current on the perception of a given oscillatory phenomenon and 2) to compare the observed features with the ones schematized in Section 3.

For what concerns spectral analysis computations, an 8-day period with respect to a 4-month record is a relatively long period. The vartious FFT analyses were done with 2, 3, 4, 6 and 12 pieces so as to be sure that the results obtained with a fine resolution

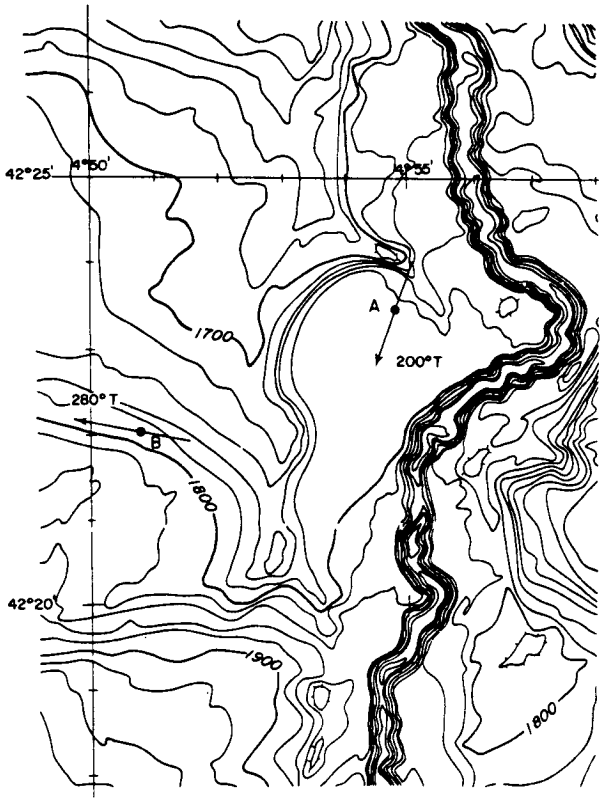


FIG. 4. The Seabeam bathymetric chart in the studied area (from Bellaiche *et al.*, 1983). The arrows represent the 4-month mean small scale currents at points A and B which are both located at ~1790 m. The Petit-Rhône canyon is structured as a mountain valley: the crest on the western side of the valley reaches ~1700 m between A and B, the bottom of the valley is flat (~1800 m near A) and the river bed is represented by a U-shaped and ~100 m deep furrow, of which the hydrodynamical regime is unknown.

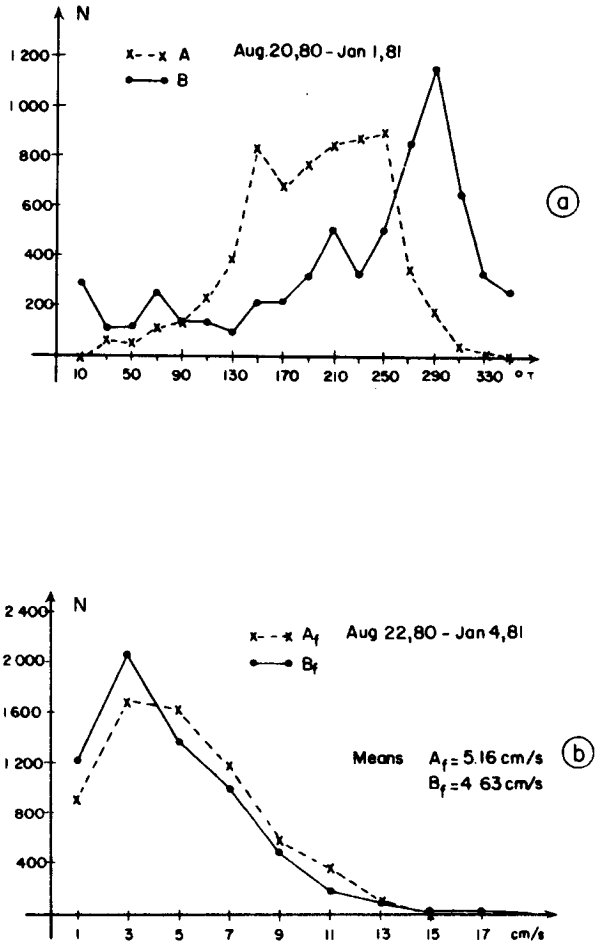


FIG. 6. Histograms at A (dashed) and B (solid). The direction-histograms (a) were computed from the original time series while the speed-histograms (b) were computed from daily time series (inertial currents-filter). *N* is the number of values.

in frequency are statistically significant. All the spectra reveal a peak between 200 and 180 h, namely at a period of about 8 days; one of the most significant peak, obtained with 4 pieces of 810 h in length, is drawn in Fig. 10a. But a satisfying accuracy for cross-spectral analyses computations is only reached for 6 pieces at least: as shown by the corresponding auto-spectra (Fig. 10b) and two-sided spectra (Table 1), the values are, from a statistical point of view, the same at both points.

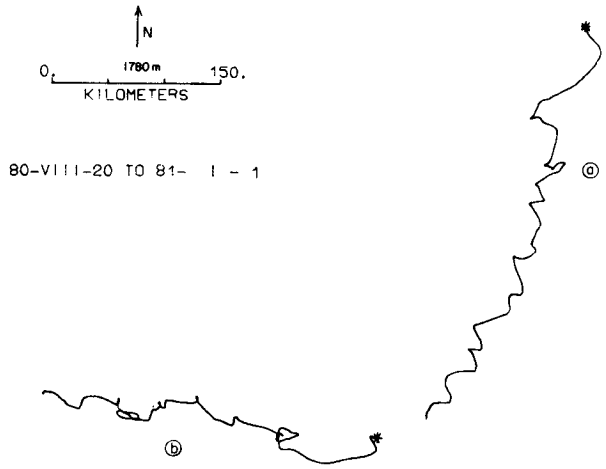


FIG. 5. The progressive vector diagrams at A (a) and B (b) from 20 August 1980 (*) to 1 January 1981.

An important result from Table 1 is that the ellipses, with respect to a rather large rotary coefficient of 0.6–0.7 (this coefficient equals 1 for a pure rotative motion and 0 for a pure rectilinear one), are remarkably stable. Indeed, an ellipse stability (which is analogous to a coherence) of 0.85–0.90 for 12 degrees of freedom (dof) is highly significant (at 95%).

Another important result is that the major axes of both ellipses have the same orientation; in this case, the 95% confidence interval for the orientation is ±15° (Jenkins and Watts, 1968, Fig. 9.3). In agreement with the spectral analyses performed with dif-

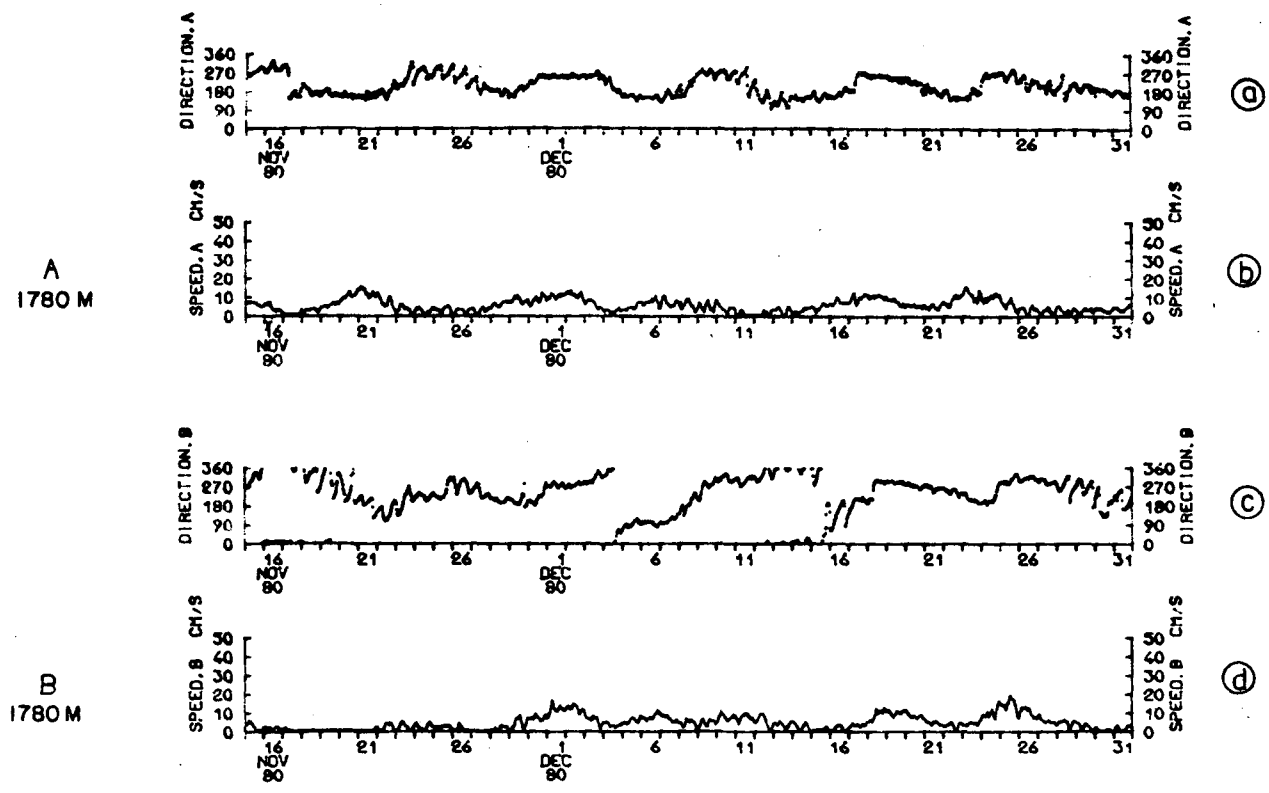


FIG. 7. Time series representative of the whole records at A (direction: a, speed: b) and B (direction: c, speed: d).

ferent numbers of pieces and for suitable forthcoming computations, a characteristic value of 125°T will be retained.

When computing the two-sided cross-spectra with 6 pieces, the coherence and the phase between the clockwise components at 180 h are 0.94 and −25° (the confidence interval is thus ±5°), (Fig. 10c). The same coefficients computed between the anticlockwise components are 0.65 (relatively low because the signal itself is low) and +25°. Therefore it is assumed that roughly the same ellipse is observed at points A and B with a typical period of 190 ± 10 h and a typical phase lag of 25 ± 5°. On an average, A leads B by about 13 h: the ranges expected for the period and the phase lag lead to a time lag of 10–16 h.

Current measurements were obtained in the surroundings, mainly on the upper part of the continental slope and in the vicinity of 42°N, 5°E, but during other periods of time, with the technical and financial support of either the CNEXO or the CFP, (Fig. 3). Features comparable to the A and B ones were observed only in the CA records collected 4 km westward from B in April–May 1981, at 75, 100, 200, 600 and 1760 m. Figure 11 shows that the directions recorded at 600 and 1760 m during the period May 1–6 are very similar: the current first slowly turns on the left and then, a few days later at the end of May 4, the direction displays a rapid clockwise change by about 90°. These features clearly look like the ones observed at A during the period 11–18 December for instance (Fig. 7a, b and 8a). During other periods of time, CA records do not show recognizable features. Due to the short length of the April–May CA records (33 days), the spectral analysis results (with 2 pieces) are not accurate; nevertheless, there is a roughly significant peak at about 8 days. In this frequency band, a signal is displayed over the entire depth with a comparable structure (Table 2): therefore, it is assumed that the wave observed at A and B has a large vertical extension, at least in the order of 1000 m. Also, the bottom intensification of the current suggested by Fig. 11 seems to be statistically supported; some aspects of the Rhines' (1970) bottom-trapped wave model will be tested later. Nevertheless and for what concerns the schematization proposed in Section 3, the motion is assumed to be basically barotropic.

*Other general features.* The infrared view taken on 27 September 1979 (Fig. 2) by TIROS-N displays the major dynamical features of the region. The Ligurian Current has a width of 40–50 km and it mainly drags surface waters, as deep as ~400 m at the coast. Velocities are 50–60 cm $s^{-1}$ in a surface layer of a few tens of meters in depth; they are ~10 cm $s^{-1}$ at 100–200 m and they smoothly decrease downwards. Westwards of 6°E, the outer edge of this current

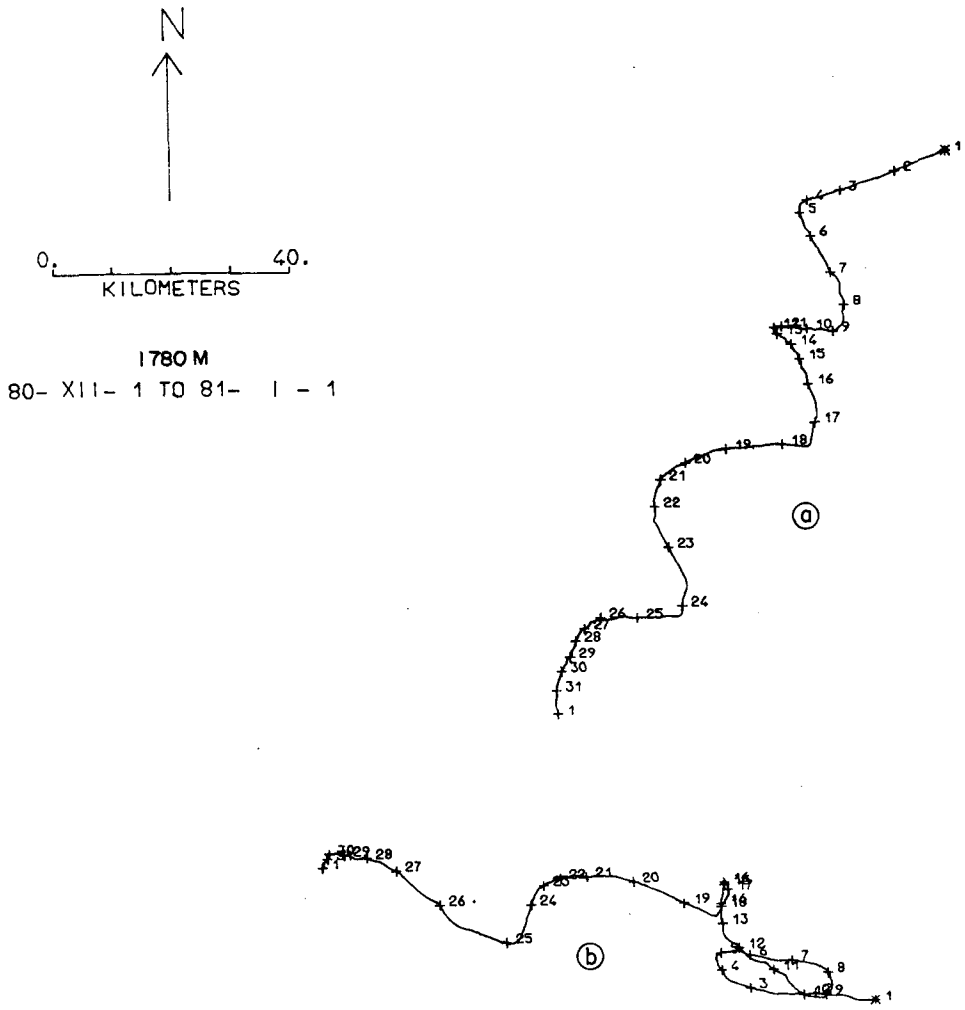


FIG. 8. Detailed sections of the progressive vector diagrams at A (a) and B (b).

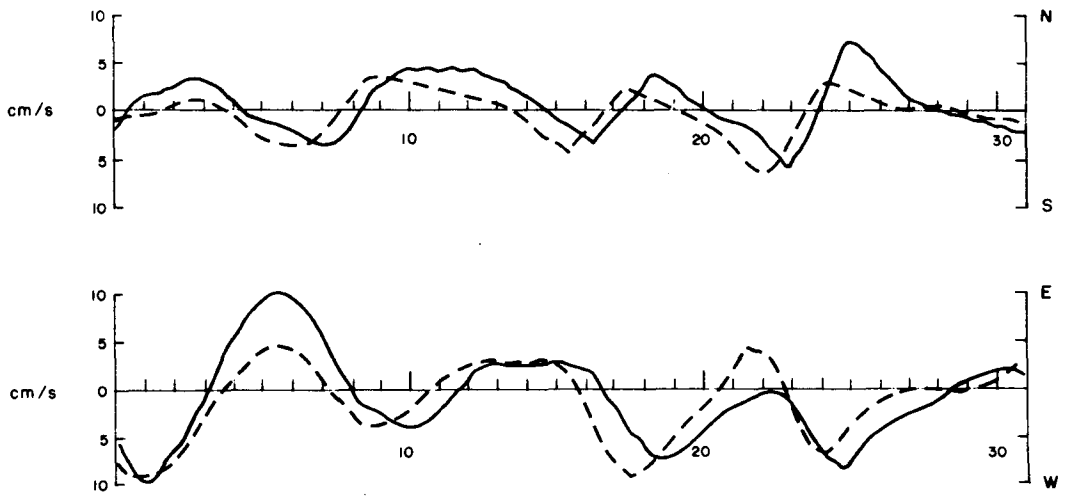


FIG. 9. Time series of the filtered E–W and N–S components at A (dashed) and B (solid). Obviously, B lags A.

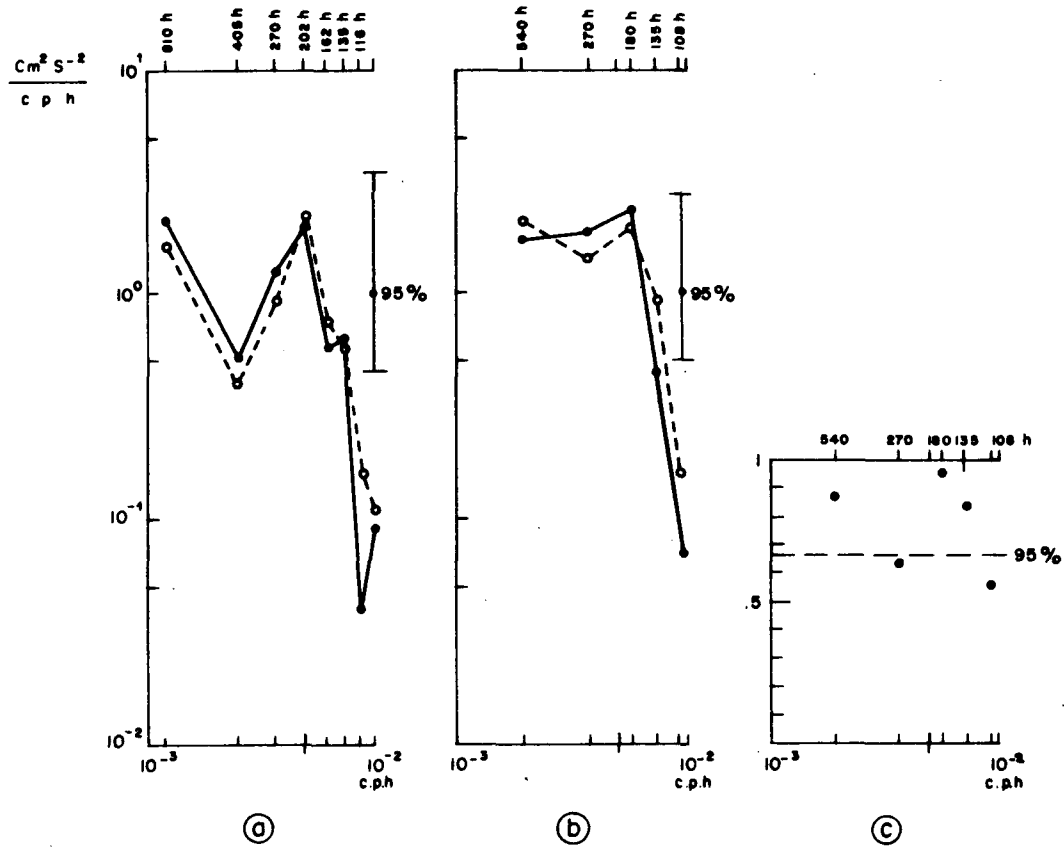


FIG. 10. A (○, dashed) and B (●, solid) clockwise autospectra with 8 dof (degrees of freedom) (a) and 12 dof (b); cross-spectrum analysis between A and B with 12 dof (c); 95% confidence limit for the test of nul hypothesis according to Koopmans (1974).

presents a wave-like structure; along the shelf break in the Gulf of Lions, the inner edge of the current presents the same wavy form thus showing that the whole current is affected by large meanders. In this region, most of the wavelength values, deduced from the analysis of several tens images, are within 60 ± 20 km. The mean phase velocity is in the order of +10 cm $s^{-1}$ (westwards) but up to +20 cm $s^{-1}$ or negative values are sometimes computed. Eastwards of 6°E, wavelengths ranging from 40 km (the phase velocity was +20 cm $s^{-1}$; Crépon *et al.*, 1982) to 120 km were described and commonly attributed to baroclinic instability of the Ligurian Current.

The analysis of the satellite imagery clearly shows that the outer edge of the current, defined with the sea surface temperature gradient, never crosses the segment CB–CE (Fig. 2). Therefore, the mean general circulation is expected to be low at ~40 km southwards in the vicinity of A, B and CA. Also, an analysis of all the current time series collected around 42°N, 5°E (a data set which represents about two years in length) shows that daily averaged speeds below the thermocline rarely exceed 15 cm $s^{-1}$ and that there is no prevailing direction.

Near the coast of Provence and along the upper part of the continental slope in the Gulf of Lions, three water masses, namely the surface water (the Ligurian Current) down to ~400 m, the intermediate (Levantine) water down to ~800 m and the bottom

TABLE 1. The two-sided spectrum analysis of records A and B with 12 dof at 180 h (enclosed by estimators at 270 and 135 h).

| Points | Clockwise spectrum $(cm\ s^{-1})^2$ | Anticlockwise spectrum $(cm\ s^{-1})^2$ | Total spectrum $(cm\ s^{-1})^2$ | Rotary coefficient | Ellipse stability | Mean orientation (°T) |
|---|---|---|---|---|---|---|
| A | 1.95 | 0.52 | 2.47 | 0.58 | 0.91 | 130 |
| B | 2.24 | 0.36 | 2.59 | 0.73 | 0.84 | 128 |

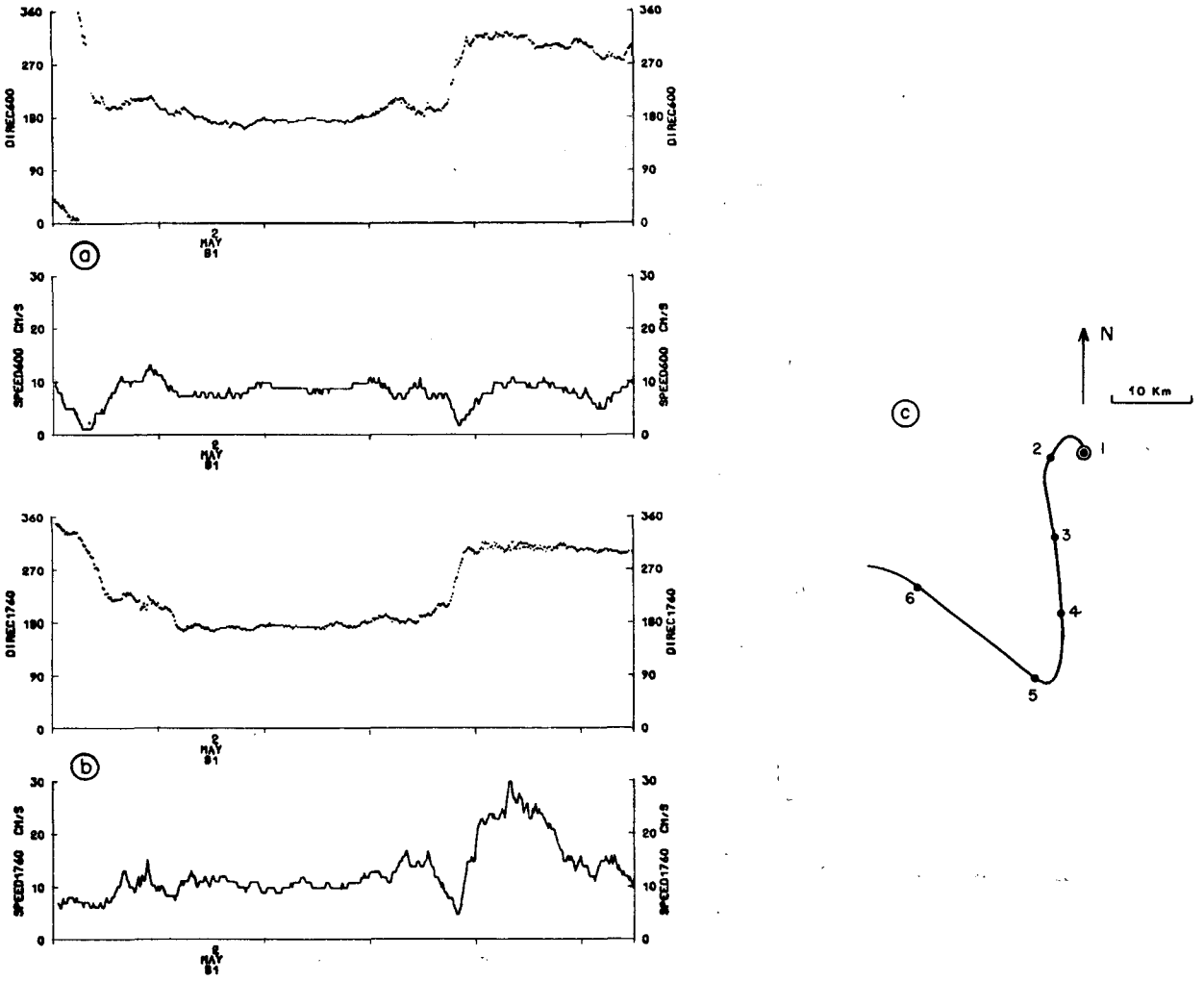


FIG. 11. Pieces of CA records on 1–6 May: direction and speed at 600 m (a) and 1760 m (b) and progressive vector diagram at 1760 m (c).

water (mainly formed during winter in the vicinity of 42°N, 5°E) can be separated by $\theta$–$S$ diagrams but the density profiles are relatively smooth (Fig. 12). These waters have densities in the order of 28.8, 29.08 and 29.11 respectively, although large spatial and temporal variations obviously occur in the surface layer; Brunt–Väisälä frequencies are in the order of a few $10^{-3}$ $s^{-1}$ in the surface layer, and a few $10^{-4}$ $s^{-1}$ downwards. Around 42°N, 5°E, the stratification is very weak and the seasonal variations are not very important; typically, $N \sim 2 \times 10^{-3}$ $s^{-1}$ between ~100 and 500 m, and $N \sim 3 \times 10^{-4}$ $s^{-1}$ below 1000 m. Therefore, records A, B and CA were actually collected in an almost homogeneous area.

The northwestern Mediterranean Sea has a complex bathymetric structure (Fig. 1). At the upper levels (0–

TABLE 2. The two-sided spectrum analysis of the CA records with 4 dof at 192 h (enclosed by estimators at 384 and 128 h).

| Depth cm $s^{-1}$ | Clockwise spectrum (cm $s^{-1}$)$^2$ | Anticlockwise spectrum (cm $s^{-1}$)$^2$ | Total spectrum (cm $s^{-1}$)$^2$ | Rotary coefficient | Ellipse stability | Mean orientation (°T) | Coherence at <0 frequency |
|---|---|---|---|---|---|---|---|
| 75 | 5.45 | 1.65 | 7.10 | 0.54 | 0.73 | 106 | ~1.00 |
| 100 | 7.68 | 1.92 | 9.60 | 0.60 | 0.59 | 99 | ~1.00 |
| 200 | 6.37 | 1.33 | 7.70 | 0.65 | 0.50 | 92 | ~1.00 |
| 600 | 7.38 | 1.94 | 9.30 | 0.58 | 0.34 | 83 | ~0.99 |
| 1760 | 10.92 | 3.03 | 13.95 | 0.57 | 0.33 | 127 | |

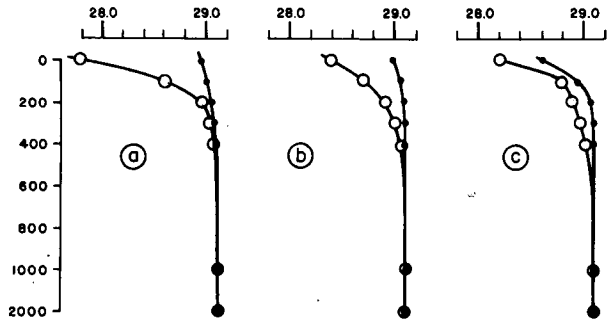


FIG. 12. Mean density profiles obtained at 6–7°E in the core of the Ligurian Current (O) and in the weakly stratified area near 42°N, 5°E (●) in November–December (a), January–February (b) and April–May (c).

1500 m), the gentle continental slope off the Gulf of Lions contrasts with the steep slope along the coast of Provence. At the lower levels (1500–2500 m), the deep-sea fan associated to the Petit-Rhône canyon is a large sedimentological edifice; upstream from A and B (i.e., towards the northeast), the bottom slope is relatively regular. In order to make simple calculations, some typical bathymetric profiles (P1 to P4 in Fig. 1) are schematized in Fig. 13. These profiles are in a direction perpendicular to the 2000-meter isobaths which are supposed to roughly guide the averaged deep circulation in the vicinity of A and B. The mean values of the slope between ~1500 and 2300 m decrease from several $10^{-1}$ at P1 to $4 \times 10^{-2}$ at P2, $3 \times 10^{-2}$ at P3 and $1.5 \times 10^{-2}$ at P4; therefore, it is assumed that the waters encountered in the vicinity of A, B and CA have flown (between P3 and P4) in a region of ~50 ± 10 km wide where the mean slope is $\sim 2 \pm 0.5 \times 10^{-2}$.

## 3. A topographic wave model

The phase lag between records A and B proves that the 8-day signal is due to a progressive phenom-

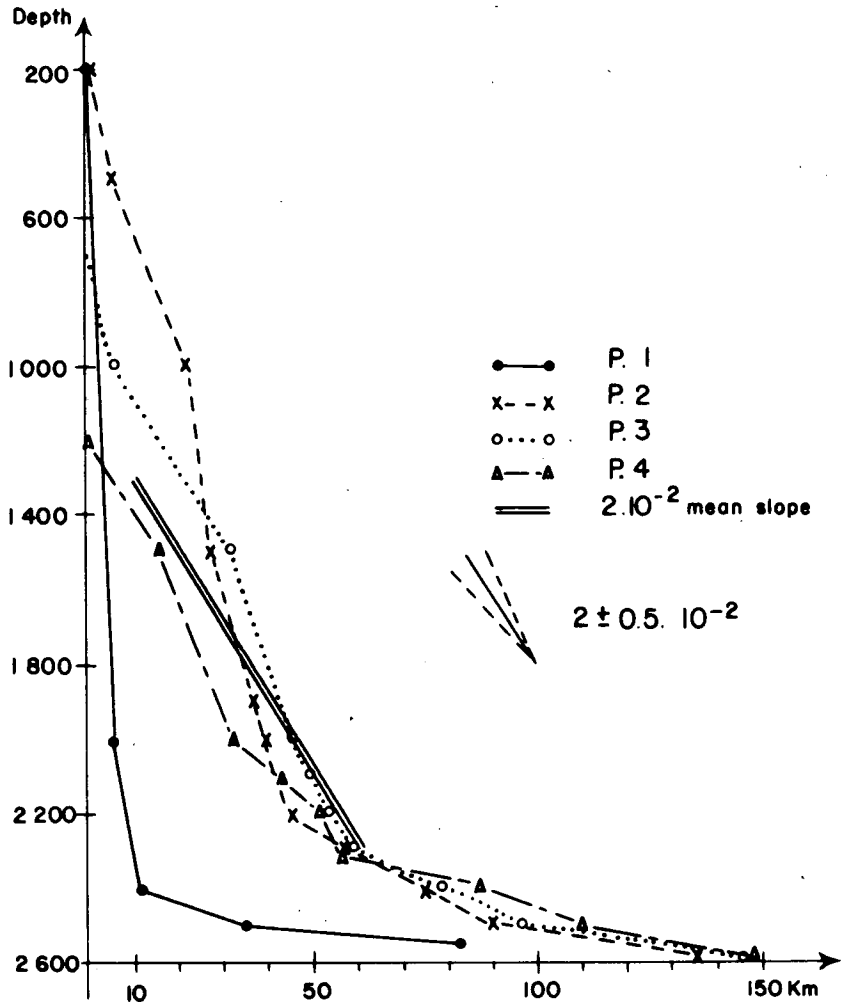


FIG. 13. Bathymetric profiles as defined in Fig. 1 and the characteristic $2 \pm 0.5 \times 10^{-2}$ bottom slope.

enon which *a priori* can be either a wave or the advection by the general circulation of specific structures, eddies for instance; why the advection of eddies cannot be supported by the data will be indicated later.

The progressive vector diagrams show that one must take into account the local bathymetry while the two-dimensional spectral analysis indicates that the 8-day phenomenon itself is not influenced by such small scale bottom features. In-phase CA signals, recorded at 600 and 1760 m, support a large vertical extension and a basically barotropic structure. Considering the location of the moorings and the space and time scale of the signal leads us to take into account the large scale slope of the bottom.

Continental shelf waves were not investigated because the visual and spectral analyses of the records collected in the upper part of the continental slope (Fig. 3) do not reveal features similar to those observed in the lower part of the slope. Also, the whole continental slope has a complex structure which cannot easily be considered in theoretical models.

As mentioned in the former sections, the Ligurian Current is located at several tens of kilometers away, and the wave propagates in quiet and weakly stratified water; also, it will be shown that nothing can be definitively concluded about the effect of the stratification. Therefore, the guiding idea was to consider a topographic wave propagating in a homogeneous fluid. As suggested by the forthcoming analysis, the wave is expected to propagate alongslope, but this direction is not the only one for topographic waves: for instance, data recorded by an array of current meters on the continental margin off Nova Scotia (Louis *et al.*, 1982) support the seaward propagation of such waves.

### *a. The theoretical background*

As a primary analysis of this oscillatory phenomenon, we have considered the free oscillations able to propagate in a $f$-plane channel with a sloping bottom (Pedlosky, 1979). As shown later on, this model leads to relatively simple relationships between the various parameters and it has been found as efficient as more sophisticated ones. For instance, the slopes without vertical walls considered by Rhines (1969) and Pedlosky (1979) lead to dispersion relationships very similar to the ones for the channel model; also, a constant bottom slope looks as representative as an exponentially varying depth. Typical parameters for the studied area clearly show that the $\beta$-effect is dominated by the topographic one.

The channel of width $L$ is infinite in length; the depth is $H_0 = D_0(1 - sy/L)$ subject to $s \ll 1$, $\overrightarrow{Oy}$ upslope. To the lowest order, the dynamical fields for the topographic wave in a homogeneous fluid are given by (Pedlosky, 1979, Eq. 3.10.15):

$$U = -\frac{g}{f}\frac{m\pi}{L} n_0 \cos(m\pi y/L) \cos(kx - \sigma t),$$

$$V = -\frac{g}{f} k n_0 \sin(m\pi y/l) \sin(kx - \sigma t),$$

where the phase speed in the $\overrightarrow{Ox}$ direction is

$$C_x = \frac{\sigma}{k} = -\frac{sf}{L}(k^2 + m^2\pi^2/L^2 + 1/R^2)^{-1}.$$

The amplitude of the surface oscillation is $n_0$, $R^2 = gH_0/f^2$, while the other parameters are classically defined. With $U_0 = \pi g/fL$, $V_0 = k/f$, and $\sigma < 0$, the current time series recorded at ($x = 0$, $y = y_0$) will be

$$U = -U_0 n_0 \cos(\pi y_0/L) \cos\sigma t,$$

$$V = +V_0 n_0 \sin(\pi y_0/L) \sin\sigma t$$

for the first mode. Higher modes have not been considered because they do not satisfy the conditions required by our hypotheses and by the observations (see Section 3b). A major advantage of this model is that the structures of the theoretical currents make possible the analytical formulation of quantities used in spectral analysis computations (Hunt, 1975). For instance, the anticlockwise and clockwise rotation parameters $A$ and $C$, which are related to the corresponding spectra by $S_A = \frac{1}{2}AA^*$ and $S_C = \frac{1}{2}CC^*$, are defined by

$$A = -\frac{n_0}{2}[+U_0 \cos(\pi y_0/L) + V_0 \sin(\pi y_0/L)],$$

$$C = +\frac{n_0}{2}[-U_0 \cos(\pi y_0/L) + V_0 \sin(\pi y_0/L)].$$

The orientation of the ellipse equals $\theta = \frac{1}{2}(\arg A + \arg C)$ and the rotary coefficient is defined by $\Omega = (S_C - S_A)/(S_C + S_A)$. A critical value for the ellipse orientation is

$$\alpha = \frac{1}{\pi}\arctan(U_0/V_0):$$

- if $y_0/L < \alpha$ or $y_0/L > (1 - \alpha)$, then $\arg A = \arg C = \pi$ or 0 and $\theta = \pi$ or 0;
- if $\alpha < y_0/L < (1 - \alpha)$, then $\arg A = \pi$, $\arg C = 0$ and $\theta = \pi/2$;
- if $y_0/L = \alpha$ or $1 - \alpha$, either $A$ or $C = 0$ and $\theta$ is undefined.

Thus, only two orientations can be observed: in the central part of the channel (respectively, near the channel sides), the major axis of the ellipse is perpendicular (parallel) to the sides, i.e., perpendicular (parallel) to the direction of propagation. The rotary coefficient is $\Omega = \Omega_0[-\sin(2\pi y_0/L)]$, with $\Omega_0(U_0, V_0, y_0) > 0$. The motion is purely rectilinear (i.e., $\Omega = 0$) at $y_0/L = 0$, 0.5 and 1. It is purely rotative at $y_0/L = \alpha$ (respectively $1 - \alpha$): there, $S_C$ ($S_A$) equals 0 and

$\Omega = -1$ (+1). Elsewhere, $\Omega$ is >0 (<0) in the shallower (deeper) half part of the channel. Therefore, the results of the channel model can be efficiently tested with the current data but several problems were masked.

First of all, this model forces the wave to travel alongslope while in the more realistic case of a horizontally-unbounded fluid, the dispersion relation considers two wavenumbers, $k$ and $l$: the case for a constant bottom slope was solved by Pedlosky (1979); Eq. 3.15.5: $\sigma = -(sf/L)k/(k^2 + l^2 + R^{-2})$ and that for an exponentially varying depth by Rhines (1969); Eq. 2.3: $\sigma = fGk/(k^2 + l^2 + F^2/4)$ where $G = (1/E - F)$, $1/E = \beta/f \sim O$ in the case of a negligible $\beta$-effect and $F = h_y/h$). Basically, these relationships have similar structures: if the wave actually propagates alongslope, this argues for the validity of the channel model. If the direction of propagation is markedly different, the available data do not allow the study of the phenomenon and the forthcoming analysis is completely erroneous. But several arguments support the alongslope direction of propagation: these are the specific relationship between the orientation of the large scale bottom slope and that of the ellipses (Section 3b), and especially the similarity between the features observed and those schematized according to such an hypothesis (Section 3c).

Secondly, the theoretical $U$ and $V$ time series, formerly expressed, indicate that no mean current is induced by the wave. Now, mean small scale currents are observed at the two points along the local isobaths: they reveal the occurrence of a mean large scale flow ($\overrightarrow{Um}$) whose effect on the wave must be estimated. The general case is difficult to solve, but simple results were obtained with a uniform flow streaming alongslope, which is expected to be the case in the studied area ($\overrightarrow{Um} = -\overrightarrow{Um}\mathbf{Ox}$, ($\overrightarrow{Um} > 0$). Thus, the phase speed in a direction parallel to the isobaths is defined by the relationship $C_x = (\overrightarrow{Um} - (sf/L + (\overrightarrow{Um}/R^2)/(k^2 + l^2 + R^{-2})$, (Pedlosky, 1979, Eq. 3.18.9). The comparison of Eq. 3.18.9 and Eq. 3.15.5 shows that the first effect of the flow is a Doppler shift and that the second effect is an alteration of the phase speed.

The baroclinic structure for the topographic wave is not considered in a basic state. Only rough estimations will be made with the CA records; the dispersion relation for constant bottom slope $\tau$ and stability frequency $N$ (Rhines, 1970) is $\sigma = \tau N \sin\theta \times \coth(kNH/f)$, where $\theta$ is the angle between $k$ and upslope while the horizontal velocity components are proportional to $\cosh(kNz/f)$, $\overrightarrow{Oz}$ upwards.

### b. *A quantitative analysis of the observations*

At a horizontal length scale of some tens of kilometers, Fig. 1 shows that the mean orientation of the whole isobaths in the studied area, between P2 and P4 (upstream from A and B), is 210–220°T (typically 215°T). The right angle with the major axis of the ellipses (125 ± 15°T, Table 1), although perhaps fortuitous, is noteworthy. If actual, such a specific angle supports a simple relationship between the mean slope and the wave: the leading hypothesis, later supported by other arguments, is that the wave travels alongslope. In these conditions, the channel model is relatively efficient (Section 3a); $\theta$ being equal to $\pi/2$, both points are expected to be located in the central (and largest) part of the virtual channel, and moreover $\Omega$ being positive, in the shallower half. Extrapolating to an actual wave which propagates alongslope within a limited depth range, this means that A and B are well within the depth range and on the right side of the wave path.

Points A and B are separated by 6.2 km in the 245°T direction, that is a separation of 5.4 km for a wave traveling towards 215°T. A phase lag of 25° induced by such an 8-day wave leads to a mean phase speed $C_x = -11$ cm s$^{-1}$; the range for the time lag (13 ± 3 h) estimated in Section 2 leads to a phase speed of 9–15 cm s$^{-1}$. In order to estimate the effect of the mean flow on the wave, we need to know it at a large space and time scale. As deduced from the A, B and CA records, the year-to-year variability is large; therefore, the mean flow during the period of interest has to be estimated with the A and B records only. The mean flow in the studied area is expected to be along the mean isobaths upstream from A and B (towards 215°T); the mean current computed at A being 3.3 cm s$^{-1}$ towards 200°T (roughly in the direction expected for the mean flow), an expected value for the mean flow is ~3 cm s$^{-1}$.

The mean flow (3 cm s$^{-1}$) is a significant percentage of the phase speed (11 cm s$^{-1}$): it induces a non-negligible Doppler shift, but the structure of the wave is not altered (Section 3a). The phase speed relative to the mean flow (and its range deduced from that of the time lag estimated in Section 2) is thus ~8 cm s$^{-1}$ (6 to 12 cm s$^{-1}$); the proper period is ~11 days (12.5 to 9.5 days) and the associated wavelength is ~78 km (65 to 95 km). It is fundamental to note that an accurate description of such a wave is linked to a significant estimation of the mean flow and that a variable mean flow completely masks such waves.

The virtual channel was defined in Section 2 by characteristic values: a width $L = 50$ km, a slope parameter $\beta = 2 \times 10^{-2}$, a maximum depth $D_0 = 2300$ m and $f = 10^{-4}$ s$^{-1}$. With $R^{-2} \ll \pi^2/L^2$ and a phase speed of 8 cm s$^{-1}$, the relationship $k^2 = \beta f/D_0 C - \pi^2/L^2$ leads to $k = 8.3 \times 10^{-5}$ m$^{-1}$, that is a mean wavelength of 76 km. Note that $k^2 < 0$ for the second mode, which justifies the unique solution retained in Section 3a. The "lucky" equality between the observed and computed mean wavelengths has to be confirmed by confidence intervals. Ranges of ±3 cm s$^{-1}$, ±0.005 and ±10 km, for the phase speed,

the bottom slope and the channel width (Section 2) lead to ranges for the wavelength of ±22, ±15 and ±9 km respectively and ranges for the period of ±5.5, ±2 and ±1.5 days respectively. Therefore, and according to this specific analysis of the data, the channel model is found efficient to satisfyingly describe the observed phenomena.

As noticed by the reviewers, phase and group velocities of first mode are in opposite directions, which could be inconsistent with our hypothesis about the generating phenomenon (Section 4). Now, the group velocity ($d\sigma/dk$) is ~2 cm $s^{-1}$ to the northeast while the large scale mean flow is ~3 cm $s^{-1}$ to the southwest. Therefore, the observations and the model are not inconsistent with a southwestward propagation (at a very low speed) of the energy associated with the wave.

Considering the results of Rhines (1970) with $\theta = 90°$ leads to periods in the order of 5 days, which is relatively low. According to the variations with depth of the CA velocities, the theoretical ratio of kinetic energies at two depths can be computed: this ratio decreases from 1.2 (1760 m/600 m) to 1.0 (near the surface). These values compare well with the data (Table 2): although sparse, the observations over the whole depth are not inconsistent with a bottom intensification of the currents due to the stratification. Observations comparable to ours (wavelength, period, vertical structure, orientation of the major axis) were made by Thompson and Luyten (1976) in the vicinity of site D. They found a good agreement with the model of Rhines, but the computations they performed with the temperature measurements are not significant here because of the homogeneity of the deep waters.

### c. *A qualitative simulation of the observations*

Mean small scale currents at A and B, directed along the local isobaths, are obviously induced by a mean large scale flow. In Section 3b, it was assumed that the mean small scale current at A was representative of the mean large scale flow expected over the whole depth along the continental slope; this assumption was based on the fact that the direction of the local isobaths at A (200°T) was roughly similar to the direction of the large scale isobaths (215°T). The mean small scale currents do not influence the wave itself, but they give a distorted image of the wave: in this subsection, we show that considering such a wave plus a mean small scale current represents fairly well the observed specific features.

The typical parameters defined in Section 3b ($k = 8.3 \times 10^{-5}$ $m^{-1}$, $L = 50$ km) indicate that $U_0/V_0 = \pi/(kL) = r \sim 0.7$. The rotary coefficient $\Omega$, which is a function of $U_0$, $V_0$ and $y_0/L$ according to the model, is 0.5–0.7 according to the data; corresponding values for $y_0/L$ are either 0.65 or 0.92 (this second value is unsuitable because it is $>1 - \alpha$ which corresponds to a major axis of the ellipse parallel to the isobaths). Ranges of ±10 km, ±10 km, ±0.1 for the width of the channel, the wavelength and the rotary coefficient lead to ranges of ±0.2 and ±0.05 for $U_0/V_0$ and $y_0/L$ respectively. The computed ordinate of both points (0.65 ± 0.05) is comparable to the ordinate (0.5) of the 1800 m isobath in a virtual channel defined by a width of 50 km and a maximum depth of 2300 m.

Let us now consider the theoretical time series defined in Section 3a. With $P > 0$ proportional to the amplitude of the wave, $I$ and $J$ being the components of the mean small scale current (in cm $s^{-1}$, $I_a = -3.19$, $J_a = -0.85$, $I_b = -1.10$ and $J_b = +2.36$), and $\sigma$ being the absolute value of the apparent frequency, the recorded time series will be $U(t) = P \times \cos\sigma t + I$ and $V(t) = \delta P \sin\sigma t + J$, with $\delta = r^{-1} \tan(\pi y_0/L) \sim -3$. The spectral analysis gives an energy density in a large frequency band and thus $P$ cannot be computed directly from the data. Figure 5a shows that $U(t)$ at A is always negative which leads to $P < -I_a \sim 3$ cm $s^{-1}$. The simulation of the time series with values for $P$ in the range 0–3 cm $s^{-1}$ is pretty well representative of the observed features; the results now discussed were obtained with $P = 2$ cm $s^{-1}$ and $T = 190$ h.

Figures 14a, b display the progressive vector diagrams computed at A and B during the time interval $(0, T)$. Starting at $t = 0$, the current at A slowly turns to the left, then the speed increases, the current turns to the right and the cycle begins again; at B the current slowly rotates clockwise (it slowly turns to the left when $P$ is relatively low), keeps a constant direction during a short time, turns to the right, the speed reaches its maximum and the cycle begins again. The theoretical time series of the velocity components at the two points are obviously similar, but the time series of the velocity and of the direction are very different. The direction-histograms (Fig. 14c) show two peaks of similar magnitude at A; these peaks are 120° apart and no value is computed outside the interval (150–270°T). At B, two elementary peaks are displayed, the larger one at 300°T and the smaller one at 140°T (160° apart); all the directions are more or less encountered at B. The velocity histograms at A and B (Fig. 14d) display averaged values of 5.28 and 4.65 cm $s^{-1}$, and maxima of 7.6 and 8.4 cm $s^{-1}$; at A one observes a peak centered at 5–7 cm $s^{-1}$ while at B, a narrower peak is centered at lower values; lower and higher values are more frequent at B than at A. Comparing these features with those described in Section 2 clearly shows that the simple assumption of a mean small scale current plus a large scale wave is pretty well representative of the observed phenomena; consequently, the hypothesis of a wave propagating alongslope is reinforced.

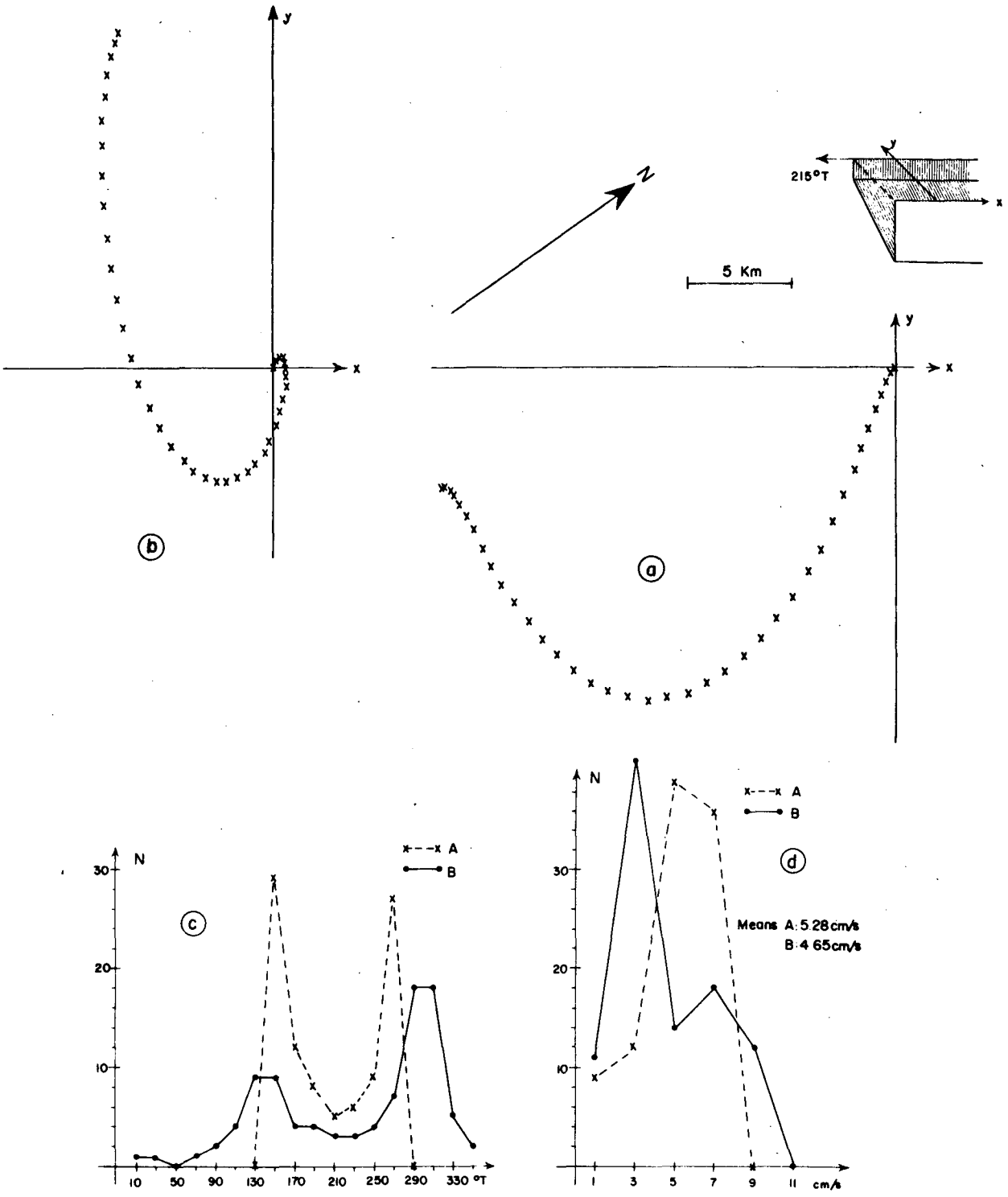


FIG. 14. Progressive vector diagrams computed at A (a) and B (b) during one period. Direction histograms (c) and speed histograms (d) computed at A (dashed) and B (solid).

## 4. Discussion

Some discrepancies obviously exist between observed and simulated features. The first fact to emphasize is that the theoretical diagrams were computed with statistical values of the parameters; but one has to be convinced that each specific period of observation can be simulated in a better way with specific

values of the parameters. For instance, increasing the mean local currents with respect to the current induced by the wave causes, among other things, the two peaks to be closer in the direction histograms; at A, the trough between the peaks will be filled up while at B, the difference between the height of the peaks will become larger. Notice that such a situation, which leads to theoretical diagrams more similar to the observed ones, is also encountered if the mean local currents are more permanent than the wave. As expected, the rapid clockwise turning which normally occurs for a few hours is not well simulated: the real phenomena are obviously much complicated.

It was mentioned in Section 2 that the CA features resemble the A ones only at certain times. Notice that CA is located far from the axis of the deep-sea fan towards the southwest. The large scale flow and/or the propagating wave, both directed towards the southwest on the northeastern side of the fan, are expected to be markedly disturbed by the great change in direction undergone by the isobaths in the axis of the fan. It is therefore expected that the time series and the progressive vector diagrams display varying features.

It was indicated at the beginning of Section 3 that the observed phenomena are not in agreement with the advection of an eddy by a large scale flow. According to the structure of the eddy, one can compute theoretical diagrams which more or less resemble the A ones, but difficulties arise when the mean small scale current markedly differs from the large scale flow (as at B). Also, the magnitude of the large scale flow equals the phase velocity in the direction of the flow, and the extrema of the recorded speed equal the magnitude of the flow plus or minus the current due to the eddy: such a scenario is not supported by the data. Note that when the mean flow and the eddy-current are of the same order, it is possible to define, with one current time series and according to this simple model, what kind of eddy (cyclonic or anticyclonic) was advected on this or that side of the observer; this is not possible if the mean flow is relatively low (Pietrafesa and Janowitz, 1979).

The various data sets described in the former sections clearly support the occurrence of an 8-day propagating phenomenon, its confinement in the vicinity of the 2000 m isobath and its extension over a great depth. No appropriated source of energy being expected in this so-called "quiet area," we have to look for a forcing mechanism in an area from where the wave comes: as a first attempt to go further into the understanding of this mechanism, two hypotheses were tested.

The first one deals with interactions between the deep waters and the topography. It is well known that the deep waters flow southwestwards along the coast of Provence and Fig. 1 shows that the mean orientation of the deeper isobaths markedly changes in a critical area centered near 42°50'N, 5°30'E. Therefore, the deep waters impinging on the continental slope westwards of 6°E are expected to receive potential vorticity which is able to further destabilize the flow and, as a possible event, generate topographic waves. In this case, the oscillations of the surface isotherms (Fig. 2) are not directly related to the forcing mechanism; but several features, such as the occurrence of undulating isotherms far from the critical area, are not easily explained. Besides, no theoretical model is available and therefore, this phenomenon can hardly be investigated.

The second hypothesis deals with unstable processes which are expected (Section 2) to affect the Ligurian Current along the coast of Provence. According to this hypothesis a scenario can be outlined: a westward propagating wave is forced in the deep layer, it is trapped by the bottom topography and then, in the critical area mentioned in the former paragraph, it is deflected southwestwards in the quiet and homogeneous region. Current measurements and detailed CTD sections have been obtained since late 1981 near 7°E. These data sets will probably allow an accurate study of the stability of the Ligurian Current.

Therefore, the several-day period and the phase lag between the records at A and B easily convince everybody of the occurrence of a propagating phenomenon. The specific relationship between the orientation of the currents induced by the wave and the bottom slope, and especially the similarity between the features observed and those schematized with the simple model account for the occurrence of a topographic wave. The Ligurian Current is expected to be involved in the generation of the wave, but nothing has been demonstrated about the forcing mechanism.

*Acknowledgments.* Obtaining and processing the various data sets was made possible with the support of several organisms: the Centre d'Essais de la Mediterranée (CEM), the Centre National pour l'Exploitation des Océans (CNEXO), the Centre National de la Recherche Scientifique (CNRS), the Centre de Télédétection et d'Analyse des Milieux Naturels (CTAMN), and the Compagnie Française des Pétroles (CFP). M. Crépon, Pr. H. Lacombe, L. Wald and two anonymous reviewers made helpful suggestions; the author also wishes to thank A. Lamy for help in processing the current data and I. Taupier-Letage for help in improving the English language.

## REFERENCES

Bellaiche, G., P. Orsolini, B. Petit-Perrin, J. L. Berthon, C. Ravenne, V. Coutellier, L. Droz, J. C. Aloïsi, H. Got, Y. Mear, A. Monaco, J. M. Auzende, P. Beuzart and S. Monti, 1983: Morphologie au sea-beam de l'éventail sous-marin profond du Rhône (Rhône deep-sea fan) et de son canyon afférent. C. R. Acad. Sc., t.286, sér. 2, 579–583.

Crépon, M., L. Wald and J. M. Monget, 1982: Low-frequency waves in the Ligurian Sea during December 1977. *J. Geophys. Res.*, **87**(C1), 595–600.

Fieux, M., 1972: Contribution à l'étude hydrologique et dynamique du Golfe du Lion en période hivernale. Thèse 3ème cycle, Paris VI, 90 pp.

Gascard, J. C., 1977: Quelques éléments de la dynamique de formation des eaux profondes méditerranéennes. Thèse d'Etat, Paris VI, 147 pp.

Hunt, M., 1975: TIMSAN analysis program. Int. Rep. Woods Hole Oceanographic Institution, 194 pp.

Jenkins, G. M., and D. G. Watts, 1968: *Spectral Analysis and its Applications.* Holden-Day, 525 pp.

Koopmans, L. H., 1974: *The Spectral Analysis of Time Series.* Academic Press, 366 pp.

Louis, J. P., B. D. Petrie and P. C. Smith, 1982: Observations of topographic Rossby waves on the continental margin off Nova Scotia. *J. Phys. Oceanogr.*, **12**, 47–55.

Millot, C., 1978: Wind induced upwellings in the Gulf of Lions. *Oceanol. Acta*, **2**(3), 261–274.

——, 1981: La dynamique marine du plateau continental du Golfe du Lion en été. Thèse d'Etat, Paris VI, 53 pp.

——, and L. Wald, 1980: The effect of the Mistral wind on the Ligurian Current near Provence. *Oceanol. Acta*, **3**(4), 399–402.

——, and A. Monaco, 1984: Deep intense currents and sedimentary transport in the northwestern Mediterranean Sea. *Geo-Marine Lett.*, **4**, 13–17.

Pedlosky, J., 1979: *Geophysical Fluid Dynamics.* Springer-Verlag, 624 pp.

Pietrafesa, L. J., and G. S. Janowitz, 1979: A note on the identification of a Gulf Stream spin off eddy from eulerian data. *Geophys. Res. Lett.*, **6**(7), 549–552.

Rhines, P., 1969: Slow oscillations in an ocean of varying depth. Part 1: Abrupt topography. *J. Fluid Mech.*, **37**(1), 161–189.

——, 1970: Edge-, bottom- and Rossby waves in a rotating stratified fluid. *Geophys. Fluid Dynamics*, **1**, 273–302.

Thompson, R. O. R. Y., and J. R. Luyten, 1976: Evidence for bottom-trapped topographic waves from single moorings. *Deep-Sea Res.*, **23**, 629–635.